

Pb_{10-x}Cu_x(PO₄)₆O: a Mott or charge transfer insulator in need of further doping for (super)conductivity

Liang Si^{a,b}, Markus Wallerberger^b, Andriy Smolyanyuk^b, Simone di Cataldo^b, Jan M. Tomczak^{b,c}, and Karsten Held^b

^a School of Physics, Northwest University, Xi'an 710127, China

^b Institute of Solid State Physics, TU Wien, 1040 Vienna, Austria

^c Department of Physics, King's College London, Strand, London WC2R 2LS, United Kingdom

(Dated: August 11, 2023)

We briefly review the status quo of research on the putative superconductor Pb₉Cu(PO₄)₆O also known as LK-99. Further, we provide *ab initio* derived tight-binding parameters for a two- and five-band model, and solve these in dynamical-mean-field theory. The ratio interaction-to-bandwidth makes LK-99 a Mott or charge transfer insulator. Electron or hole doping (which is different from substituting Pb by Cu and thus differs from LK-99) is required to make it metallic and potentially superconducting.

I. INTRODUCTION

In recent preprints^{1,2}, Lee, Kim, *et al.* reported the discovery of a room-temperature superconductor at ambient-pressure: Pb_{10-x}Cu_x(PO₄)₆O with $0.9 < x < 1.1$. They had previously named this material LK-99 after their initials and the year of the first synthesis. Their more recent samples show somewhat stronger signatures of superconductivity¹⁻³: (i) a sharp drop in the resistivity^{2,3}, according to Ref. 1 to the order of $10^{-10} - 10^{-11}$ Ωcm though in Refs. 2 and 3 a higher noise level is visible, (ii) a negative (diamagnetic) spin susceptibility and levitation on a magnet², and (iii) sharp voltage jumps at critical currents, with the critical currents vanishing in approximately a quarter-circle as a function of temperature and magnetic field^{1,3}.

If LK-99 is truly a superconductor at ambient temperature and pressure, it is arguably one of the most significant physics discoveries of recent history. However, experimental confirmation is urgently needed: The above experiments, while indicative of superconductivity, do not unambiguously prove it. (i) The noise level of the resistivity appears too large for concluding that LK-99 has zero resistance. (ii) The negative susceptibility and levitation can be caused by a simple diamagnet. (iii) The voltage jumps might also be caused by contact issues. One has to admit however that taken everything together, the overall picture provides quite some indication for superconductivity. If the critical temperature was 1 K [and if taking into account the first confirmations of (i) and (ii), see below], the scientific community would now most likely be quite positive that at least parts of the LK-99 sample are superconducting. But room temperature superconductivity is an extraordinary claim, and extraordinary claims rightfully require an extraordinarily solid proof. Such waterproof evidence has not been given as of the time of submitting this article, neither has solid evidence against.

Naturally, the results by Lee, Kim *et al.* led to huge experimental and theoretical efforts. Let us briefly review the status quo of these subsequent works as of the day of submission (Aug. 8th, 2023): The levitation (i) has been

reproduced by Wu *et al.*⁴ and further groups on social media. A sharp drop in resistivity has been confirmed by Hou *et al.*⁵, albeit at 100 K instead of 100° Celsius. Hou *et al.* also report two strange resistivity jumps above 250 K (which the authors suggest might be caused by issues with the electrode contacts) as well as an abnormal field dependence.

In contrast, other experimental groups report an opposite behavior. Liu *et al.*⁶ find an increase of the resistivity with decreasing temperature indicating that LK-99 is a semiconductor or insulator. They also observe a paramagnetic response instead of a diamagnetic one, and the magnetic susceptibility as well as the resistivity increases with decreasing temperature. Kumar *et al.*^{7,8} also successfully synthesized Pb_{10-x}Cu_x(PO₄)₆O in a modified lead apatite structure, and report a diamagnetic insulator. Abramiam *et al.*⁹ conjecture that the samples by Lee *et al.* are not pure LK-99, but a coexistence of superconducting and non-superconducting regions; superconductivity might emerge from another material. Guo *et al.*¹⁰ report a ferromagnetic hysteresis and half levitation.

As for theory, density functional theory (DFT)¹¹ is state-of-the-art for calculating crystal structures and for getting, at the bare minimum, a first idea of the electronic structure. Five groups¹²⁻¹⁶ independently performed such DFT calculations, appearing on arXiv within days, and showing similar results (cf. 8,17,18): For the lead apatite crystal structure with one Pb atom replaced by Cu, two very flat bands cross the Fermi energy. Below these are still flat, but slightly more dispersive O bands, and another Cu band. Some of the DFT calculations also analyze possible alternative Cu and O positions^{13,14,16,18} so far to a very limited extent; Cabezas-Escases¹⁶ find an instability with a simplified frozen phonon calculation. Lai *et al.*¹² suggest that gold-doped lead apatite may have stronger effects than Cu. Griffin¹³, Si and Held¹⁴, and Kurlita *et al.*¹⁵ argue that the flat bands might boost electron-phonon mediated superconductivity; Si and Held¹⁴ also suggest purely electronic flat-band superconductivity¹⁹⁻²¹ as a possible alternative.

Some groups^{12,13,15,16} consider the flat DFT bands crossing the Fermi energy as evidence that Cu doping

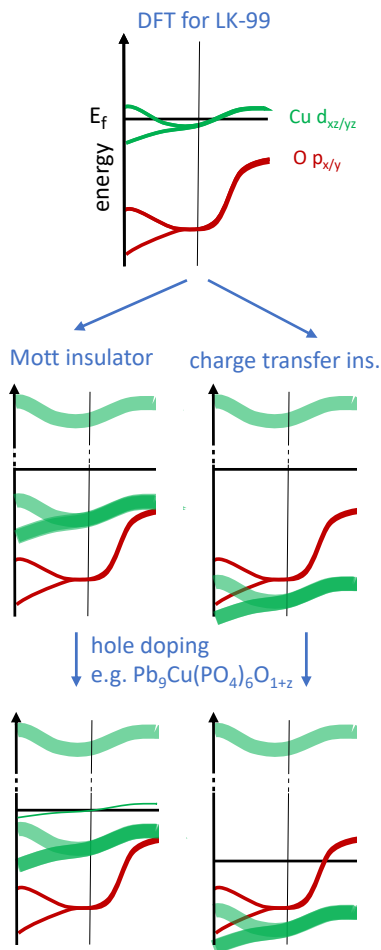


FIG. 1. Top: Schematics of DFT bandstructure for $\text{Pb}_9\text{Cu}(\text{PO}_4)_6\text{O}$. Middle: Mott-Hubbard splitting of the Cu $d_{xz,yz}$ orbitals leading to a Mott or charge transfer insulator. Note here we visualize the case with an orbital symmetry breaking (ordering) indicating by having different orbitals in the lower and upper Hubbard band. Interrupted lines indicate a larger energy separation. Bottom: if doped the Mott or charge transfer insulator becomes metallic. here hole doping is visualized. For electron doping the quasiparticle band (and Fermi energy) would be closer to the upper Hubbard band. A charge transfer insulator for electron doping is not plausible, because the next unoccupied orbitals (Pb p) are too high in energy¹⁴.

$x \approx 1$ makes insulating lead apatite metallic, thus explaining the conducting and prospectively superconducting state of LK-99. While this is suggestive from the DFT results, Si and Held¹⁴ estimate the interaction-to-bandwidth U/W to be of $\mathcal{O}(10)$ and thus conclude that LK-99 must be a Mott (or charge transfer) insulator, see Fig. 1 for an illustration. They further conjecture that the accompanying spin-1/2 should show a strong paramagnetic response so that a diamagnet without superconductivity is difficult to imagine.

Indeed such a Mott²² or charge transfer²³ insulator might explain the simultaneous experimental findings of

a paramagnetic insulator. At the same time, the metallic (and prospectively superconducting) behavior found in the other experiments^{1–5} is possible if (part of) the sample is doped, see Fig. 1 (bottom). Indeed high-temperature cuprate superconductors²⁴ are in the same class of a charge transfer (or Mott) insulator²⁵, and also have Cu and O orbitals as the relevant ones. However, this is how far the similarity goes. Superconducting cuprates have U/W only of $\mathcal{O}(1)$, and the Cu atoms form a square lattice in the CuO_2 planes, while the lead apatite crystal structure is hexagonal. To make such a Mott or charge transfer insulator metallic, one needs electron or hole doping which is not possible by changing x , i.e., the ratio of Cu:Pb. The synthesis procedure² and lead apatite crystal structure suggests that electron doping was possible for $0 < y \ll 1$ and $z < 0$ and hole doping for $z > 0$ in $\text{Pb}_{10-x}\text{Cu}_x(\text{P}_{1-y}\text{S}_y\text{O}_4)_6\text{O}_{1+z}$. Note, the nominal oxidation states are: Pb^{2+} , Cu^{2+} , P^{5+} , S^{6+} and O^{2-} . Anyhow, this is merely an educated guess.

Also based on the picture of a doped Mott insulator, Baskaran²⁶ speculates that Cu atoms cluster in chains or 2D patches with a Cu^0 electronic configuration instead of Cu^{2+} ^{12–16}, and thus realize his theory of a broad band Mott localization. First groups also started doing calculations for two-orbital models on a triangular lattice, using a Bardeen, Cooper and Schrieffer (BCS)²⁷ type of coupling²⁸ and slave-boson mean field theory. The authors find f -wave and s -wave superconductivity (though at too low critical temperatures)²⁹, respectively.

In this paper, we would like to put such tight binding parameters on a more solid basis. To this end, we do a Wannier function projection and calculate the tight binding parameters for: (i) a two-band low energy model made up of the Cu $d_{xz/yz}$ orbitals and (ii) a five-band model also involving the O $p_{x/y}$ states just below these and, additionally, the next Cu (d_{z^2}) orbital, see Fig. 1 (top) [this Fig. does not include the 3rd Cu d orbital below the O $p_{x/y}$ bands, cf. Fig. 2 below]. These tight-binding models can be used for subsequent many-body calculations and are listed in I and II, respectively. We motivate the strength of the Kanamori interaction parameters on the Cu sites. Finally we solve these models in DMFT and find a Mott or charge transfer insulator. A similar insulator is also obtained in DFT+ U , but only if the crystal symmetry lifts the degeneracy of the Cu $d_{xz/yz}$ orbitals.

Let us put some caveats here regarding the low-energy model. It assumes the periodic continuation of a unit cell with a single formula unit ($x = 1$, $y = 0$, $z = 0$) and optimized O and Cu positions¹⁴. This yields among others, a regular triangular lattice of the Cu sites. Other O and Cu positions are, however, so close in energy¹⁴ that we must expect a disordered arrangement of these at room temperature — unless there is a crystal distortion stabilizing some arrangement. The x-ray diffraction (XRD) patterns^{2,5,6} clearly indicate an undistorted lead apatite structure without periodic arrangement of the Cu atoms. For the matter of Mott insulator or not, this is not rele-

vant, but for (super)conductivity the possible long-range ordering of the Cu and O atoms or vice versa a disordered arrangement of these is very relevant.

II. COMPUTATIONAL METHODS

DFT-level structural relaxations and static calculations are performed by employing VASP^{30,31} and WIEN2K^{32,33} code with the Perdew-Burke-Ernzerhof version for solids of the generalized gradient approximation (GGA-PBESol)³⁴ and a dense $9 \times 9 \times 13$ k -mesh for the unit cell of $\text{Pb}_9\text{Cu}(\text{PO}_4)_6\text{O}$. The relaxed ground state crystal structure is shown in Fig. 2(a). The two low-energy effective Hamiltonians are generated by projecting the derived DFT bands, now computed by WIEN2K, around the Fermi level onto Wannier functions^{35,36} using WIEN2WANNIER^{37,38}. The real-space Wannier Hamiltonian is then transformed to momentum space using a \mathbf{k} -mesh with 18,125 reducible points.

For the DMFT calculations, this DFT-derived one-particle Hamiltonian is supplemented by a local Kanamori interaction on the Cu sites, see Section III, and we employ the fully localized limit as double counting correction scheme³⁹. $O-p$ orbitals are considered as non-interacting. We solve the resulting many-body Hamiltonian at room temperature (298 K, $\beta = 1/(k_B T) = 39 \text{ eV}^{-1}$) within DMFT employing a continuous-time quantum Monte Carlo (QMC) solver in the hybridization expansions⁴⁰ using W2DYNAMICS^{41,42}. Real-frequency spectra are obtained with the ANA_CONT code⁴³ via analytic continuation using the maximum entropy method (MaxEnt)^{44,45}.

Further, the rotationally invariant DFT+ U scheme⁴⁶ with $U = 3 \text{ eV}$ and $J = 0.7 \text{ eV}$ on top of the regular PBE^{47,48} functional as implemented in the VASP package was employed for DOS and bandstructure calculations for two representative relaxed crystal structures. The plane wave cutoff is 600 eV, $4 \times 4 \times 5$ and $5 \times 4 \times 4$ k -mesh was used for $P3$ (143) and Pm (6) structures. AFLOW-SYM⁴⁹ was used for the symmetry analysis.

III. TIGHT BINDING MODELS

The two-band and five-band tight binding model consist of $m = 1.2$ and $m = 1.5$ orbitals in the unit cell, respectively. For the two-band model these are the d_{xz} and d_{yz} orbitals of the Cu-site, for the five-band model there are two additional O p_x and p_y orbitals from oxygen sites and one more d_{z^2} orbital from the Cu-site. This motif is periodically extended on a hexagonal k -grid. This tight-binding Hamiltonian \mathcal{H}^0 is supplemented by a local Coulomb interaction term \mathcal{H}_{int} on the Cu sites.

$$\mathcal{H} = \mathcal{H}^0 + \mathcal{H}_{int}. \quad (1)$$

For the non-interacting part

$$\mathcal{H}^0 = \sum_{\mathbf{k}, \sigma, m, n} \mathcal{H}_{m,n}^0(\mathbf{k}), \quad (2)$$

we set up a tight-binding parametrization

$$\mathcal{H}_{m,n}^0(\mathbf{k}) = \sum_{i,j} t_{im,jn} e^{i\mathbf{k}(\mathbf{R}_i - \mathbf{R}_j)} c_{i,m\sigma}^\dagger c_{j,n\sigma}, \quad (3)$$

where $c_{i,m\sigma}^\dagger$ ($c_{i,m\sigma}$) is the creation (annihilation) operator, and i, j indicate unit cells $\mathbf{R}_i, \mathbf{R}_j$, while m, n are orbital indices, and σ the spin index. For the interaction part,

$$\mathcal{H}_{int} = \sum_{i, \sigma, \sigma'} \mathcal{H}_{int}^{\sigma, \sigma'}(i) \quad (4)$$

we use the Kanamori form

$$\begin{aligned} \mathcal{H}_{int}^{\sigma, \sigma'}(i) = & U \sum_m n_{m,\sigma} n_{m,\sigma'} \\ & + \sum_{m>n} [U' n_{m,\sigma} n_{n,\sigma'} + (U' - J) n_{m,\sigma} n_{n,\sigma'}] \\ & - \sum_{m,n} J (d_{m,\sigma}^\dagger d_{n,\sigma'}^\dagger d_{n,\sigma} d_{m,\sigma'} + d_{m,\sigma}^\dagger d_{m,\sigma'}^\dagger d_{n,\sigma} d_{n,\sigma'}), \end{aligned} \quad (5)$$

where all number operators, $n_{m,\sigma}$, act on the same Cu site (i.e., are in the same unit cell i), and the m, n orbitals are restricted to the two and three Cu orbitals for the respective two- and five-band model, defined below.

A. Two-band tight-binding model

As only two bands cross the Fermi energy, our initial objective is to establish a two-band model for $\text{Pb}_9\text{Cu}(\text{PO}_4)_6\text{O}$. As depicted in Fig. 2(a,b), the bands intersecting at the Fermi level (E_f) primarily arise from the Cu d_{yz} and d_{xz} orbitals (in the coordinate system with z aligned with the c unit cell vector). Thus, a minimal low-energy model with only these two orbitals appears possible. It can facilitate subsequent calculations that extend beyond the scope of DFT, as fewer orbitals require less computational resources for complicated many-body calculations. The energy range chosen for this two-band Wannier projections is -0.1 eV to 0.1 eV. Fig. 2(c) shows the excellent fit of the bands in the Wannier gauge to the DFT. Truncating the hopping amplitudes at the second nearest neighbors, yields the hopping elements collected in Table I.

It is worth noting that, due to the presence of a trigonal distortion, the orthogonality between d_{yz} and d_{xz} bands, which is preserved in an undistorted CuO_6 octahedron, is lifted. The distortion itself can be best seen in Fig. 2(b). It leads to the emergence of non-zero hopping terms such as the nearest neighbor (t_1) hopping from $e_g(1)$ to $e_g(2)$

Orbital-1	Orbital-2	t_{000}	t_1	t_1	t_1	t_1	t_1	t_1	t_2	t_2	t_2	t_2	t_2	t_2	t_z
		(000)	(100)	(010)	(110)	(-1-10)	(-100)	(0-10)	(120)	(210)	(1-10)	(-1-20)	(-2-10)	(-110)	(001)
$e_g(2)$	$e_g(2)$	-24	6	-5	0	0	6	-5	0	0	0	0	0	0	-10
$e_g(1)$	$e_g(1)$	-24	-6	5	0	0	-6	5	0	0	0	0	0	0	-10
$e_g(2)$	$e_g(1)$	0	6	4	-2	15	-11	-13	0	0	0	0	0	0	0
$e_g(1)$	$e_g(2)$	0	-11	-13	15	-2	6	4	0	0	0	0	0	0	0

TABLE I. Two-band model, comprising two Cu $e_g(1)$ and $e_g(2)$ orbitals (corresponding to d_{yz} , d_{yz}). Hopping parameters up to second nearest from Cu to Cu sites and Orbital-1 to Orbital-2. Here, t_1 and t_2 denote 1st and 2nd nearest hoppings. The numbers in brackets indicate the hopping vector in real space, see Fig. 3(f). Hopping terms that are close to or smaller than 1 meV are put as 0 meV. All hoppings are in units of meV; t_{000} is the on-site energy.

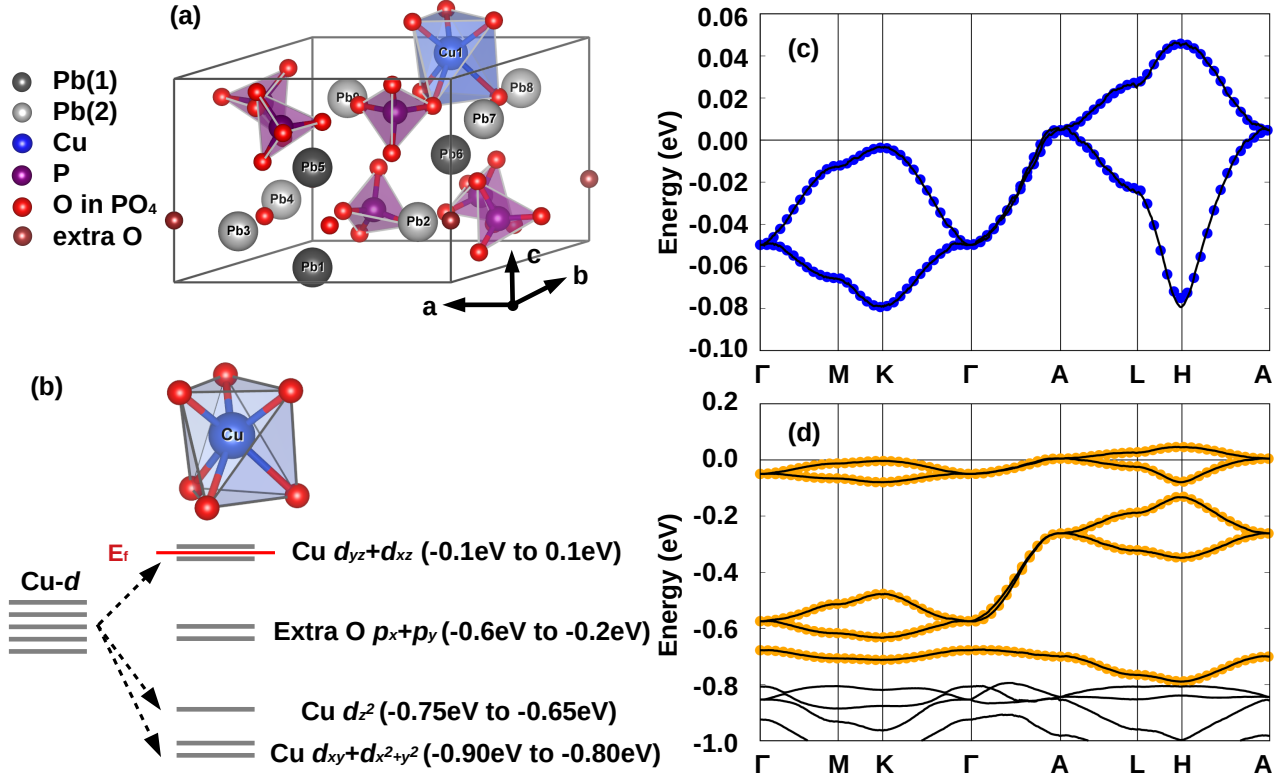


FIG. 2. (a) DFT-relaxed structure of $\text{Pb}_9\text{Cu}(\text{PO}_4)_6\text{O}$; (b) schematic figure of energy band splitting from the octahedral Cu-coordination of the CuO_6 motif; Wannier projections for the two bands model (c) and five bands model (d), respectively. The Wannier bands (dots) are virtually identical to the DFT bands (lines).

along the (110) direction. For all second nearest neighbor hoppings, the predicted values are close to zero (less than 1 meV), indicating that hopping between Cu ions in $\text{Pb}_9\text{Cu}(\text{PO}_4)_6\text{O}$ can be safely restricted to first nearest neighbors. These nearest Cu neighbors are separated in space by approximately 10 Å.

The hopping energy along the z -direction, t_z , is -10 meV. Even this hopping is notably smaller than the corresponding t_z in infinite-layer nickelates and cuprates (~ 36 meV; where the in-plane hopping is from -370 to -450 meV)⁵⁰. That is, in contrast to cuprates and nickelates, in-plane and out-of-plane hoppings are quite comparable; also the Cu-Cu distance in the z -direction is with ~ 7.4 Å similar to that in-plane ones. Altogether, we can hence conclude that LK-99 has a three dimensional elec-

tronic structure.

Furthermore, we illustrate the Fermi surface using the two-band model in Fig. 4. (The Fermi surface of the five-band model is also exactly the same as that of the original DFT). Intriguingly, the Fermi surface of LK-99 exhibits striking resemblances to that of UPt_3 ^{51–53}. In UPt_3 , the prevailing consensus attributes the emergent superconductivity to heavy fermions, rather than electron-phonon coupling. This parallel suggests that the presence of super flat bands and correlations with U/W of the order of $\mathcal{O}(10)$ might play a pivotal role in driving a transition from a normal to a superconducting state.

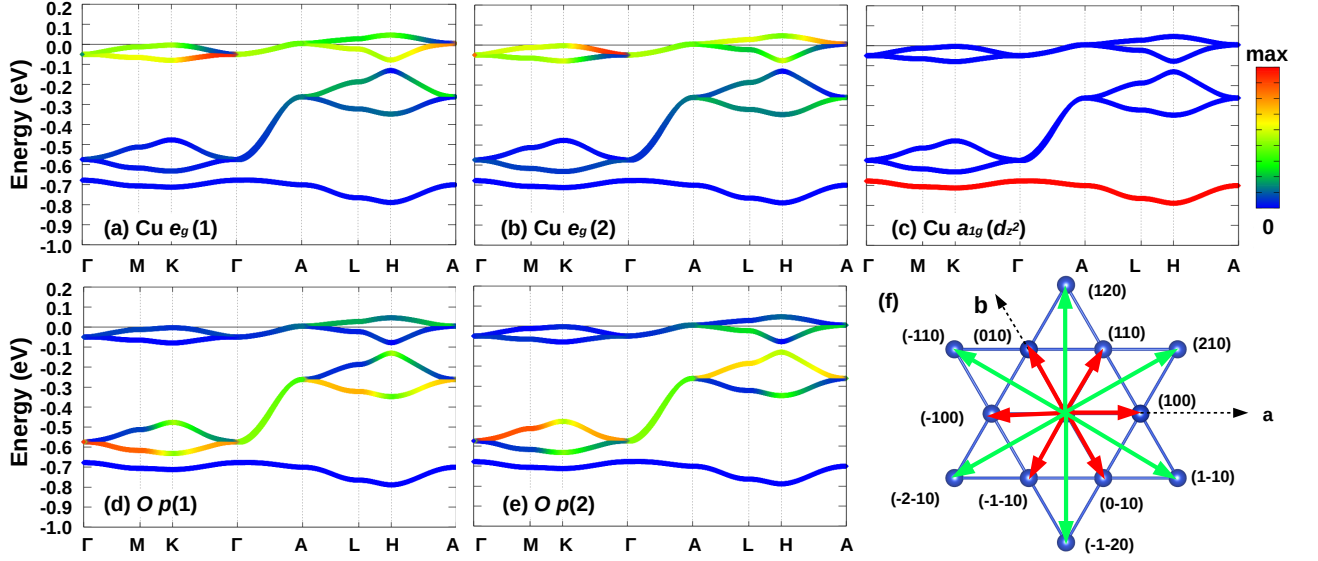


FIG. 3. Wannier bands character of (a) $e_g(1)$, (b) $e_g(2)$, (c) a_{1g} , (d) $O p(1)$, and (e) $O p(2)$. (f) Schematic hopping terms of Cu site, the red and green arrows indicate first and second nearest hopping, the numbers in bracket indicate the real space hopping vectors.

Orb-1	Orb-2	t_{000}	t_1	t_1	t_1	t_1	t_1	t_z	
		(000)	(100)	(010)	(110)	(-1-10)	(-100)	(0-10)	(001)
$e_g(1)$	$e_g(1)$	-77	0	-4	0	0	0	-4	-4
$e_g(2)$	$e_g(2)$	-77	-4	0	0	0	-4	0	-4
$e_g(2)$	$e_g(1)$	0	-4	-4	6	0	0	0	2
$e_g(1)$	$e_g(2)$	0	0	0	0	6	-4	-4	-2
$e_g(1)$	$O p(1)$	0	0	-3	0	0	3	0	0
$e_g(1)$	$O p(2)$	-7	0	0	0	-4	0	0	0
$e_g(2)$	$O p(1)$	0	0	6	2	0	5	0	0
$e_g(2)$	$O p(2)$	0	0	3	2	0	-4	0	0
$O p(1)$	$O p(1)$	-366	10	0	-11	-11	10	0	-85
$O p(2)$	$O p(2)$	-366	-10	0	11	11	-10	0	-85
$O p(2)$	$O p(1)$	0	-4	-22	15	-6	18	0	-3
$O p(1)$	$O p(2)$	0	18	0	-6	15	-4	-22	3
a_{1g}	a_{1g}	-715	6	6	6	6	6	6	12

TABLE II. Five-band model, comprising besides the two Cu e_g orbitals of the two-band model additionally two O $p(1)$ and $p(2)$ orbitals (corresponding to p_x and p_y) as well as one further Cu a_{1g} (d_{z^2}) orbital. The numbers in brackets indicate the hopping vector in real space, see Fig. 3 (f). Hopping parameters up to 1st nearest neighbor between all Cu and O sites and orbitals are given. As before, t_1 indicates 1st nearest hoppings, the numbers in brackets indicate hopping vectors in real space; hopping terms obviously smaller than 1 meV are approximated as 0 meV. The energy unit is meV.

B. Five-band tight-binding model

As the O orbitals may play an important role if LK-99 is doped with electrons or holes, see Fig. 1, we further construct a five-band model. Here, we also include the Cu d_{z^2} orbital to be on the safe side. As long as this lowest band remains firmly below the Fermi surface (i.e., is fully occupied up to hybridizations/orbital admixing),

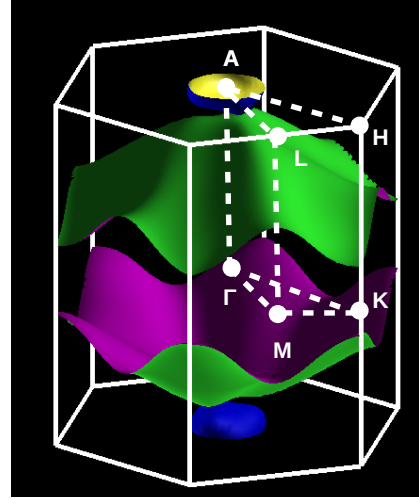


FIG. 4. (Two-band) tight-binding model Fermi surface of $Pb_9Cu(PO_4)_6O$.

it need not be considered in subsequent many-body calculations. But it can be included with a simple Hartree shift, given by the occupations (and spin polarizations) of the two Cu e_g orbitals. If on the other hand, this Cu d_{z^2} orbital accumulates holes, this is indicative that further Cu orbitals besides the two e_g orbitals need to be included in the calculation.

For this extended five-band model, the hopping parameters are detailed in Table II. In congruence with our initial analysis in Fig. 2(b) and the energy ordering displayed in Fig. 2(d), the on-site energies (t_{000}) of Cu e_g , O p , and Cu a_{1g} (d_{z^2}) orbitals amount to -77 meV, -366 meV, and -715 meV, respectively. Notably, focusing on the Cu

a_{1g} bands, we observe isotropic hoppings of the order of ~ 6 meV along all in-plane directions, while a more substantial hopping is evident along the z -direction. This consistently aligns with the inherent symmetry of the d_{z^2} orbital [Fig.2(b)]. Furthermore, as depicted in Fig.3(c), the Cu a_{1g} (d_{z^2}) band has a remarkably flat dispersion and exhibits only minimal hybridization with all other bands, *a posteriori* justifying their exclusion from a tight binding model of LK-99.

Turning to the O p orbitals in Table II, the $p(1)$ to $p(2)$ intra-orbital hoppings can reach up to 11 meV, while inter-orbital hoppings extend to -22 meV. A particularly noteworthy observation is the strong intra-orbital hopping between O p orbitals along the z -direction (t_z), amounting to -85 meV. This concurs with the pronounced dispersion of O- p orbitals along the Γ -A path, see Fig. 2(d). Considering the distance of approximately ~ 7.4 Å, such a substantial hopping is unexpected and raises the possibility of inducing anisotropic, quasi one-dimensional transport in LK-99 (if it is a charge transfer insulator, and if LK-99 is hole doped).

We can further utilize the tight-binding model for visualizing the band hybridization, by plotting the individual contribution of all five orbitals to the electronic structure. This is shown in Fig. 3. While the two Cu e_g and two O p Wannier orbitals strongly admix among themselves individually, the mixing between these two types of orbitals as well as between them and the Cu d_{z^2} orbital is weak. A notable exception is the quite strong intermixing (hybridization) between Cu d_{z^2} and O p orbitals around the H k-point. Despite the very small hopping (hybridization) between these orbitals (e.g., the Cu-O inter-orbital hopping is only $t_1(-100) = 3$ meV in Table II), the energy difference between the Cu and O bands is similarly small at momentum H. For this reason they still strongly hybridize. For example, in perturbation theory the admixture is $t_1(-100)/\Delta_H$, where Δ_H is the energy difference at H.

C. Interaction parameters

Constrained random phase approximation (cRPA)⁵⁴ calculations for other Cu- d^9 based materials^{55–58} suggest an intra-orbital Hubbard interaction $U = \mathcal{O}(2-3)$ eV for the two (three) Cu $d_{xz/yz}(+d_{z^2})$ orbitals in the 2-band (5-band) calculation. Note that the (minimal) Cu-O distance in LK-99 (2.08 Å) is longer by about 10% compared to typical cuprates, suggesting weaker hybridizations and screening. On the other hand, the bare charge-transfer energy between Cu- d and O- p orbitals, $E_d - E_p$, is much smaller than in cuprates, possibly enhancing screening effects. Further, to account for additional spectral-weight transfers from retarded processes, one typically uses a static interaction U that is enhanced with respect to the cRPA-value. Therefore, we advocate $U = 2.5 - 3.5$ eV, a Hund's exchange $J = 0.7$ eV, and an inter-orbital interaction $U' = U - 2J$. Given the flatness of the relevant

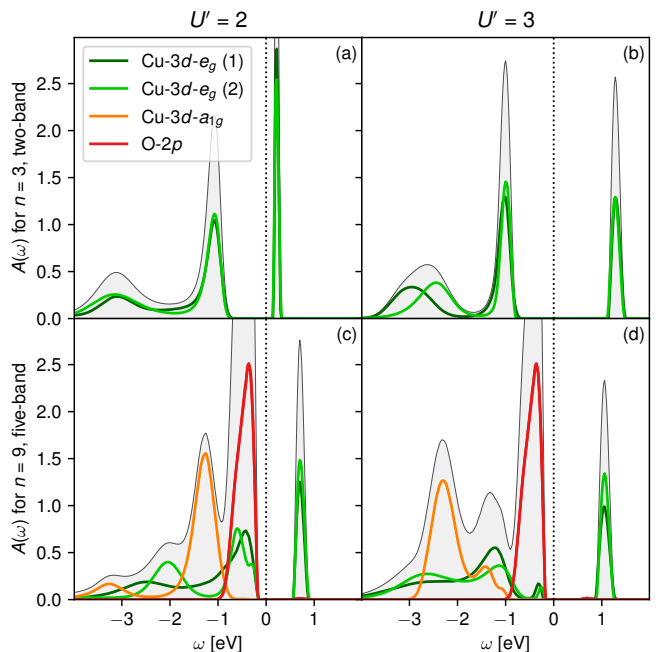


FIG. 5. Total and orbitally-resolved DMFT spectral function $A(\omega)$ for (a) the two-band tight-binding model at $U' = 2$ eV and (b) $U' = 3$ eV, as well as (c) the five-band tight-binding model at $U' = 2$ eV and (d) $U' = 3$ eV, all at $T = 298$ K.

copper bands, we expect the parent compound to be insulating for any reasonable interaction strength. The precise value will, however, be important in determining the insulating nature (Mott or charge transfer).

IV. DMFT

In order to study effects of electronic correlations on top of the tight-binding description, we perform a DMFT calculation. DMFT describes the local dynamics of electrons, by monitoring the charge (and spin) fluctuations on a given lattice site in the presence of the local Hubbard interactions. The latter, in particular, penalizes occupying a site with more than one electron per orbital and leads to a renormalization of the quasi-particle band-structure. Or, if the interaction is strong enough, to a Mott-Hubbard splitting of the DFT bands.

Fig. 5 shows the analytically-continued (to real frequencies) DFT+DMFT spectral function for both (i) the two-band and (ii) the five-band model. The (nominal) filling for the models is (i) $n = 3$ and (ii) $n = 9$ electrons per Cu site. For both models we consider two different inter-orbital interactions $U' = 2$ eV and $U' = 3$ eV, respectively, and a fixed Hund's exchange $J = 0.7$ eV; for the intra-orbital (Hubbard) interaction we use $U = U' + 2J$. The differences (uncertainties) between $e_g(1)$ and $e_g(2)$ spectra emerge since we did not enforce orbital and spin symmetry.

For both models, we see a clear gap at the Fermi en-

ergy. Both Cu e_g (i.e., d_{xz} and d_{yz}) orbitals split into a lower and an upper Hubbard band. Note that despite this Mott-Hubbard splitting, the orbital degeneracy remains. Because the system is not particle-hole symmetric, the weights of the upper and lower Hubbard bands are not symmetric.

Since the lower Hubbard band describes transitions from 3 electrons on the Cu site to 2 electrons and since 2 electrons have a singlet-triplet splitting, the lower Hubbard band has to show a multiplet splitting. Such a splitting is also seen in Fig. 5. In contrast, the transition from 3 electrons to 4 electrons, i.e., the upper Hubbard band, must not show such a splitting.

The gaps for the two-band model are larger than for the five-band models. The reason for this is that in the two-band model three more orbitals contribute to the screening, which reduces the effective interaction in a cRPA calculation. That is, we should, on the very limited U grid available and bare an actual cRPA calculation, rather compare $U' = 2$ eV for the two-band model with $U' = 3$ eV for the five band model.

As for the question of Mott or charge transfer insulator we need to look at the five-band model in Fig. 5 (c,d): At $U' = 3$ eV in Fig. 5 we clearly have a charge transfer insulator, with the first band below the Fermi energy stemming from the oxygen p orbitals. At $U' = 2$ eV we have a very strong admixture between Cu and O bands in the first spectral contribution below the Fermi energy. The system is neither a clear charge transfer nor a clear Mott insulator: We are right at the crossover between a charge-transfer to a Mott insulator. For even smaller U 's, given that this tendency continues, the system might be a Mott insulator. As we do not have interaction parameters from cRPA calculations yet, there is a *substantial* uncertainty in U ; and we cannot give a definite answer whether LK-99 is a Mott or a charge-transfer insulator. As cRPA estimations of U also have a substantial error, it might also be beyond present-day theoretical tools to decide this question.

Let us also note the small peak at -0.2 eV for $U' = 3$ eV in Fig. 5 (c). This might be akin to a Zhang-Rice singlet, see e.g.⁵⁹ for a similar peak in DFT+DMFT calculations for cuprates where such a Zhang-Rice singlet peak is visible. A difference is that, here, for LK-99, this peak is at the upper edge of the oxygen bands, not above these. Also, we should note that this small peak might be a maximum entropy artifact.

To avoid the maximum entropy uncertainties, we further present in Fig. 6 the local (\mathbf{k} -integrated) DMFT Green's function, specifically its imaginary part and now for (imaginary) Matsubara frequencies ν_n . Here $G_{\nu_n} \rightarrow 0$ for $\nu_n \rightarrow 0$ signals that there are no states at the Fermi energy, i.e., we have an insulator. Both, for $n = 9$ electrons in the five-band and $n = 3$ for the three-band model, $G_{\nu_n} \rightarrow 0$. LK-99 is an insulator.

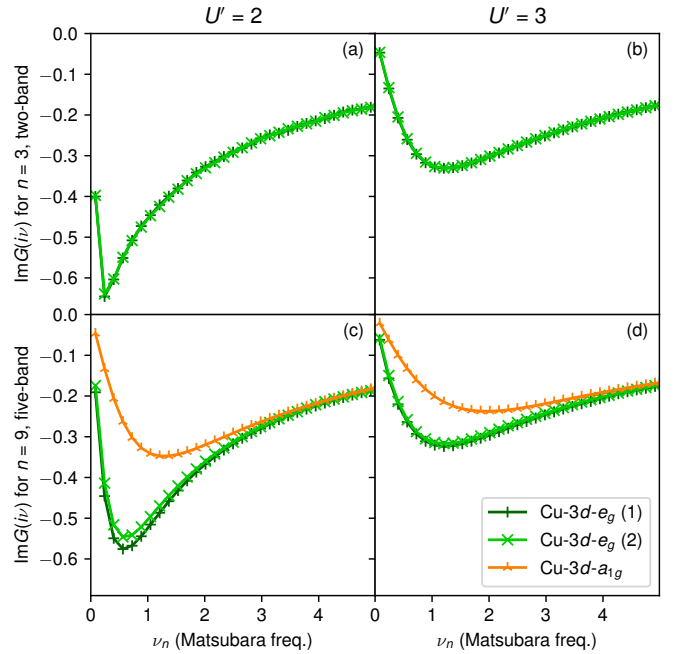


FIG. 6. Imaginary part of the local DMFT Greens function G vs. Matsubara frequency ν_n . Parameters as in Fig. 5.

V. DFT+ U

Previous DFT+ U calculations^{12,15} did not find an insulating state for the lattice symmetry and the unit cell also employed here. The degeneracy of the d_{yz} and d_{xz} orbital prevents a splitting since in DFT+ U spin or orbital polarization is needed for splitting off Hubbard bands. Our DFT+ U result of $\text{Pb}_9\text{Cu}(\text{PO}_4)_6\text{O}$ in Fig. 7(a) show the same.

However, introducing structural distortion via various positions of Cu-doping, like at Pb(2) in Fig. 2(a), further reduced system symmetry from $P3$ (143) of Fig. 2(a) to Pm (6) after DFT structural relaxations; cf. insets of Fig. 7. In this lower Pm symmetry, each Cu atom acquired four surrounding O ligands, leading to a crystal field of strongly distorted tetrahedral shape. This breaks the orbital degeneracy of the $P3$ (143) structure. In DFT+ U , see Fig. 7(b), static electronic correlations then strongly enhance the orbital splitting and additionally yield a spin polarization and a corresponding spin splitting. This ultimately gives rise to an insulating state with a similar gap as in DMFT, but here with a full spin and orbital polarization. Note that in DFT+ U E_f happens to be just below the upper Hubbard band in Fig. 7(b).

VI. CONCLUSION

To sum up, on the basis of density-functional theory, we performed a Wannier function projection for analyzing the electronic structure of $\text{Pb}_9\text{Cu}(\text{PO}_4)_6\text{O}$ (LK-

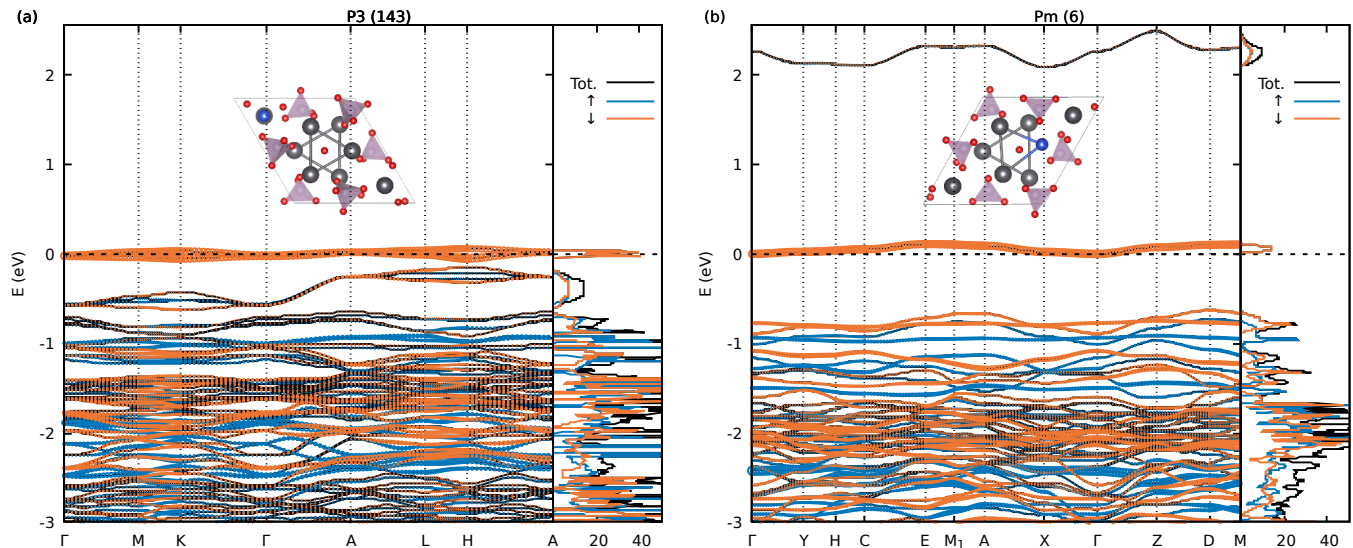


FIG. 7. DFT+ U band structure (left) and DOS (right) for two structures of $\text{Pb}_9\text{Cu}(\text{PO}_4)_6\text{O}$. Spin-up and spin-down contributions to bands (fatbands) and to DOS are highlighted in blue and orange. Panel (a) shows the calculation for the structure presented in Fig. 2(a), while panel (b) is for the structure with a different arrangement of Pb and Cu atoms (crystal structures are given in the insets with Cu and Pb atoms in blue and gray, respectively).

99). This allows for subsequent many-body calculations. Specifically, we constructed two distinct low-energy models: (i) a minimal two-band model including only the Cu d_{xz} and d_{yz} orbitals and (ii) a five-band model that additionally encompasses the O p_x and p_y orbitals as well as the Cu d_{z^2} orbital. These tight binding models shed some light on LK-99: It has a three-dimensional electronic structure of the two low-energy Cu d_{xz} and d_{yz} bands with next nearest-neighbor hoppings up to distances of 10 Å. This is contrasted with a more one-dimensional bandstructure of the O p_x and p_y orbitals; the latter orbitals can become relevant if LK-99 is a charge transfer insulator. For cuprate superconductors, higher T_c 's have been associated with smaller charge-transfer energies⁶⁰, which, there, are still of the order $\mathcal{O}(1 - 3)$ eV. This empirical trend for cuprates nicely aligns with an allegedly much higher T_c of LK-99, here, since the bare Cu-O charge-transfer energy in our five-orbital model is an order of magnitude smaller.

The ratio of interaction-to-bandwidth U/W is an order of magnitude larger than what is needed to turn a metal into a Mott insulator²². Hence, we see in DMFT a splitting of the Cu d_{xz}/d_{yz} into a lower and an upper Hubbard band so that LK-99 becomes either a Mott insulator or charge transfer insulator. Given the uncertainty in U we cannot say, at the moment, which version of these closely related insulators is realized. This splitting is a dynamical and purely electronic mechanism. In DMFT we do not observe indications for orbital or spin symmetry breaking. In contrast to DMFT, to find an

insulator in DFT+ U , a symmetry breaking of the Cu e_g (d_{xz}/d_{yz}) orbitals is required. For the crystal structure of Fig. 2(a) these are, however, degenerate. In our DFT+ U we therefore also considered a structure with Cu on the Pb(1) site in Fig. 2(a). In this case, the e_g symmetry is broken and hence the Cu bands can split into Hubbard bands, realizing an insulator also in DFT+ U .

Such a dynamic splittings into Hubbard bands and dynamical orbital reoccupations can match with likewise *dynamic* but slower Jahn-Teller phonons (lattice distortions). For example, in manganites electronic and lattice modes mutually support each other and thus localize charge carriers without symmetry breaking⁶¹. While phonons have not yet been calculated, a similar or different interplay between electron and phonon dynamics might play an important role for LK-99.

Acknowledgments We thank Robert Svagera and Neven Barišić for discussions and acknowledge funding through the Austrian Science Fund (FWF) projects I 5398, P 36213, SFB Q-M&S (FWF project ID F86), the joint project I 6142 of FWF and the French National Research Agency (ANR), and Research Unit QUAST by the Deutsche Forschungsgemeinschaft (DFG; project ID FOR5249) and FWF (project ID I 5868). L. S. is thankful for the starting funds from Northwest University. Calculations have been mainly done on the Vienna Scientific Cluster (VSC). For the purpose of open access, the authors have applied a CC BY public copyright licence to any Author Accepted Manuscript version arising from this submission.

¹ S. Lee, J.-H. Kim, and Y.-W. Kwon, [arXiv:2307.12008](https://arxiv.org/abs/2307.12008) (2023).

² S. Lee, J. Kim, H.-T. Kim, S. Im, S. An, and K. H. Auh, [arXiv:2307.12037](https://arxiv.org/abs/2307.12037) (2023).

- ³ S. Lee, J. Kim, S. Im, S. An, Y.-W. Kwon, and K. H. Auh, *J. Korean Cryst. Growth Cryst. Technol.* **33**, 61 (2023).
- ⁴ H. Wu, L. Yang, B. Xiao, and H. Chang, [arXiv:2308.01516](https://arxiv.org/abs/2308.01516) (2023).
- ⁵ Q. Hou, W. Wei, X. Zhou, Y. Sun, and Z. Shi, [arXiv:2308.01192](https://arxiv.org/abs/2308.01192) (2023).
- ⁶ L. Liu, Z. Meng, X. Wang, H. Chen, Z. Duan, X. Zhou, H. Yan, P. Qin, and Z. Liu, [arXiv:2307.16802](https://arxiv.org/abs/2307.16802) (2023).
- ⁷ K. Kumar, N. K. Karn, and V. P. S. Awana, [arXiv:2307.16402](https://arxiv.org/abs/2307.16402) (2023).
- ⁸ K. Kumar, N. K. Karn, Y. Kumar, and V. P. S. Awana, [arXiv:2308.03544](https://arxiv.org/abs/2308.03544) (2023).
- ⁹ P. Abramian, A. Kuzanyan, V. Nikoghosyan, S. Teknowijoyo, and A. Gulian, [arXiv:2308.01723](https://arxiv.org/abs/2308.01723) (2023).
- ¹⁰ K. Guo, Y. Li, and S. Jia, [arXiv:2308.03110](https://arxiv.org/abs/2308.03110) (2023).
- ¹¹ P. Hohenberg and W. Kohn, *Phys. Rev.* **136**, B864 (1964).
- ¹² J. Lai, J. Li, P. Liu, Y. Sun, and X.-Q. Chen, [arXiv:2307.16040](https://arxiv.org/abs/2307.16040) (2023).
- ¹³ S. M. Griffin, [arXiv:2307.16892](https://arxiv.org/abs/2307.16892) (2023).
- ¹⁴ L. Si and K. Held, [arXiv:2308.00676](https://arxiv.org/abs/2308.00676) (2023).
- ¹⁵ R. Kurleto, S. Lany, D. Pashov, S. Acharya, M. van Schilfgaarde, and D. S. Dessau, [arXiv:2308.00698](https://arxiv.org/abs/2308.00698) (2023).
- ¹⁶ J. Cabezas-Escases, N. F. Barrera, C. Cardenas, and F. Munoz, [arXiv:2308.01135](https://arxiv.org/abs/2308.01135) (2023).
- ¹⁷ K. Tao, R. Chen, L. Yang, J. Gao, D. Xue, and C. Jia, [arXiv:2308.03218](https://arxiv.org/abs/2308.03218) (2023).
- ¹⁸ Y. Sun, K.-M. Ho, and V. Antropov, [arXiv:2308.03454](https://arxiv.org/abs/2308.03454) (2023).
- ¹⁹ K. Kuroki, T. Higashida, and R. Arita, *Phys. Rev. B* **72**, 212509 (2005).
- ²⁰ V. I. Iglonikov, F. Hébert, B. Grémaud, G. G. Batrouni, and R. T. Scalettar, *Phys. Rev. B* **90**, 094506 (2014).
- ²¹ H. Aoki, *J. Supercond. Nov. Magn.* **33**, 2341 (2020).
- ²² F. Gebhard, *The Mott Metal-insulator transition* (Springer-Verlag (Berlin), 1997).
- ²³ J. Zaanen, G. A. Sawatzky, and J. W. Allen, *Phys. Rev. Lett.* **55**, 418 (1985).
- ²⁴ J. G. Bednorz and K. A. Müller, *Zeitschrift für Physik B Condensed Matter* **64**, 189 (1986).
- ²⁵ D. J. Scalapino, *Rev. Mod. Phys.* **84**, 1383 (2012).
- ²⁶ G. Baskaran, [arXiv:2308.01307](https://arxiv.org/abs/2308.01307) (2023).
- ²⁷ J. Bardeen, L. N. Cooper, and J. R. Schrieffer, *Phys. Rev.* **106**, 162 (1957).
- ²⁸ O. Tavakol and T. Scaffidi, [arXiv:2308.01315](https://arxiv.org/abs/2308.01315) (2023).
- ²⁹ H. Oh and Y.-H. Zhang, [arXiv:2308.02469](https://arxiv.org/abs/2308.02469) (2023).
- ³⁰ G. Kresse and J. Hafner, *Phys. Rev. B* **47**, 558 (1993).
- ³¹ G. Kresse and J. Furthmüller, *Computational materials science* **6**, 15 (1996).
- ³² P. Blaha, K. Schwarz, G. Madsen, D. Kvasnicka, and J. Luitz, An augmented plane wave + local orbitals program for calculating crystal properties (2001).
- ³³ K. Schwarz and P. Blaha, *Computational Materials Science* **28**, 259 (2003), Proceedings of the Symposium on Software Development for Process and Materials Design.
- ³⁴ J. P. Perdew, A. Ruzsinszky, G. I. Csonka, O. A. Vydrov, G. E. Scuseria, L. A. Constantin, X. Zhou, and K. Burke, *Phys. Rev. Lett.* **100**, 136406 (2008).
- ³⁵ G. H. Wannier, *Phys. Rev.* **52**, 191 (1937).
- ³⁶ N. Marzari, A. A. Mostofi, J. R. Yates, I. Souza, and D. Vanderbilt, *Rev. Mod. Phys.* **84**, 1419 (2012).
- ³⁷ A. A. Mostofi, J. R. Yates, Y.-S. Lee, I. Souza, D. Vanderbilt, and N. Marzari, *Computer physics communications* **178**, 685 (2008).
- ³⁸ J. Kuneš, R. Arita, P. Wissgott, A. Toschi, H. Ikeda, and K. Held, *Computer Physics Communications* **181**, 1888 (2010).
- ³⁹ V. I. Anisimov, J. Zaanen, and O. K. Andersen, *Phys. Rev. B* **44**, 943 (1991).
- ⁴⁰ E. Gull, A. J. Millis, A. I. Lichtenstein, A. N. Rubtsov, M. Troyer, and P. Werner, *Rev. Mod. Phys.* **83**, 349 (2011).
- ⁴¹ N. Parragh, A. Toschi, K. Held, and G. Sangiovanni, *Phys. Rev. B* **86**, 155158 (2012).
- ⁴² M. Wallerberger, A. Hausoel, P. Gunacker, A. Kowalski, N. Parragh, F. Goth, K. Held, and G. Sangiovanni, *Computer Physics Communications* **235**, 388 (2019).
- ⁴³ J. Kaufmann and K. Held, [arXiv:2105.11211](https://arxiv.org/abs/2105.11211) (2021).
- ⁴⁴ J. E. Gubernatis, M. Jarrell, R. N. Silver, and D. S. Sivia, *Phys. Rev. B* **44**, 6011 (1991).
- ⁴⁵ A. W. Sandvik, *Phys. Rev. B* **57**, 10287 (1998).
- ⁴⁶ A. I. Liechtenstein, V. I. Anisimov, and J. Zaanen, *Phys. Rev. B* **52**, R5467 (1995).
- ⁴⁷ J. P. Perdew, K. Burke, and M. Ernzerhof, *Physical Review Letters* **77**, 3865 (1996), publisher: American Physical Society.
- ⁴⁸ J. P. Perdew, K. Burke, and M. Ernzerhof, *Physical Review Letters* **78**, 1396 (1997), publisher: American Physical Society.
- ⁴⁹ D. Hicks, C. Oses, E. Gossett, G. Gomez, R. H. Taylor, C. Toher, M. J. Mehl, O. Levy, and S. Curtarolo, *Acta Crystallographica Section A* **74**, 184 (2018).
- ⁵⁰ M. Kitatani, L. Si, O. Janson, R. Arita, Z. Zhong, and K. Held, *npj Quantum Materials* **5**, 59 (2020).
- ⁵¹ A. De Visser, A. Menovsky, and J. Franse, *Physica B+C* **147**, 81 (1987).
- ⁵² J. Sauls, *Advances in Physics* **43**, 113 (1994).
- ⁵³ S. Li, Z. Tong, C. Shao, H. Bao, T. Frauenheim, and X. Liu, *The Journal of Physical Chemistry Letters* **13**, 4289 (2022).
- ⁵⁴ T. Miyake and F. Aryasetiawan, *Phys. Rev. B* **77**, 085122 (2008).
- ⁵⁵ S. W. Jang, H. Sakakibara, H. Kino, T. Kotani, K. Kuroki, and M. J. Han, *Scientific Reports* **6**, 33397 (2016).
- ⁵⁶ D. Di Sante, A. Hausoel, P. Barone, J. M. Tomczak, G. Sangiovanni, and R. Thomale, *Phys. Rev. B* **96**, 121106 (2017).
- ⁵⁷ O. Ivashko, M. Horio, W. Wan, N. B. Christensen, D. E. McNally, E. Paris, Y. Tseng, N. E. Shaik, H. M. Rønnow, H. I. Wei, C. Adamo, C. Lichtensteiger, M. Gibert, M. R. Beasley, K. M. Shen, J. M. Tomczak, T. Schmitt, and J. Chang, *Nature Communications* **10**, 786 (2019).
- ⁵⁸ F. Nilsson, K. Karlsson, and F. Aryasetiawan, *Phys. Rev. B* **99**, 075135 (2019).
- ⁵⁹ P. Hansmann, N. Parragh, A. Toschi, G. Sangiovanni, and K. Held, *New J. Phys.* **16**, 033009 (2014).
- ⁶⁰ C. Weber, C. Yee, K. Haule, and G. Kotliar, *EPL (Europhysics Letters)* **100**, 37001 (2012).
- ⁶¹ S.-L. Yang, J. A. Sobota, Y. He, Y. Wang, D. Leuenberger, H. Soifer, M. Hashimoto, D. H. Lu, H. Eisaki, B. Moritz, T. P. Devereaux, P. S. Kirchmann, and Z.-X. Shen, *Phys. Rev. B* **96**, 245112 (2017).